RESEARCH ARTICLE
SPACE PHYSICS: MAGNETOSPHERIC PHYSICS

Earth and Planetary Physics
8: 356–367, 2024
doi: 10.26464/epp2024016

The dawn–dusk asymmetry in mesosphere and lower thermosphere temperature disturbances during geomagnetic storms at high latitude

GuanChun Wei[1], JianYong Lu[1], Fen Tang[2*], JingYuan Li[1], and Meng Sun[1]

[1]Institute of Space Weather, School of Atmospheric Physics, Nanjing University of Information Science & Technology, Nanjing 210044, China;

[2]College of Information and Communication, National University of Defense Technology, Wuhan 430019, China

Key Points:

- A statistical study was performed on the dawn–dusk asymmetry of temperature perturbations in the high-latitude mesosphere and lower thermosphere during geomagnetic storms.
- During the main phase of geomagnetic storms, cooling phenomena are more prevalent on the dawn side at high latitudes than on the dusk side.
- The asymmetry in temperature disturbances between dawn and dusk is associated with the difference in vertical wind disturbances between the day and night sides.

Citation: Wei, G. C., Lu, J. Y., Tang, F., Li, J. Y., and Sun, M. (2024). The dawn–dusk asymmetry in mesosphere and lower thermosphere temperature disturbances during geomagnetic storms at high latitude. *Earth Planet. Phys.*, *8*(2), 356–367. http://doi.org/10.26464/epp2024016

Abstract: Utilizing observations by the Sounding of the Atmosphere using Broadband Emission Radiometry (SABER) instrument, we quantitatively assessed the dawn–dusk asymmetry in temperature disturbances within the high-latitude mesosphere and lower thermosphere (MLT) during the main phase of geomagnetic storms in this study. An analysis of five geomagnetic superstorm events indicated that during the main phase, negative temperature disturbances were more prevalent on the dawn side than on the dusk side in the high-latitude MLT region. Results of a statistical analysis of 54 geomagnetic storm events also revealed a notable disparity in temperature disturbances between the dawn and dusk sides. At high latitudes, 38.2% of the observational points on the dawn side exhibited negative temperature disturbances (less than −5 K), whereas on the dusk side, this percentage was only 29.5%. In contrast, at mid-latitudes, these proportions were 34.1% and 36.5%, respectively, showing no significant difference. We also conducted a statistical analysis of temperature disturbances at different altitudes, which revealed an increase in the proportion of warming disturbances with altitude. Conversely, the proportion of cooling disturbances initially rose with altitude, reaching a peak around 105 km, and subsequently decreased. These temperature disturbance differences could be explained by the day–night asymmetry in vertical wind disturbances during storm conditions.

Keywords: dawn; dusk asymmetry; SABER (Sounding of the Atmosphere using Broadband Emission Radiometry); geomagnetic storms; mesosphere and lower thermosphere

1. Introduction

During geomagnetic storms, a substantial amount of energy and an abundance of particles are injected into the polar regions, resulting in intense disturbances in the thermosphere (Wang W et al., 2008; Fejer et al., 2017). Processes such as Joule heating and thermal convection, which contribute to the temperature rise in the thermosphere, exert further influence on the middle to lower thermosphere (Banks, 1979; Roble et al., 1987), inducing temperature changes around 100 km altitude. This temperature variation is coupled with intricate physical and chemical processes in the middle to lower thermosphere, as well as the dynamics of the lower layers, making it challenging to comprehend disturbances in the mesosphere and lower thermosphere (MLT) region during storm conditions.

Numerous simulations and observational studies have been conducted on the warming of the MLT during geomagnetic storms. Roble et al. (1987) calculated the Joule heating rates for the geomagnetic storm on June 13, 1982, which coincided with a solar proton event, and found that heating rates at altitudes of 70–80 km could reach 1–3 K/d while exceeding 20 K/d above 90 km. Shefov (1968, 1969) observed the impact of geomagnetic storms on high-latitude mesospheric temperatures by measuring the rotational temperature of OH emission. Wand (1983) noted

First author: G. C. Wei, 202391000004@nuist.edu.cn
Correspondence to: F. Tang, tangfen1204@126.com
Received 12 DEC 2023; Accepted 25 JAN 2024.
First Published online 01 MAR 2024.

that during geomagnetic storms, a change in the *Kp* index from 0 to 5 could lead to a temperature increase of 18 to 47 K in the lower thermosphere between 105 and 135 km. During the magnetic storm event on June 27, 1992, Fagundes et al. (1996) used the Fabry–Perot interferometer to measure nighttime temperature averages and found these measurements to be higher than during quiet periods. von Savigny et al. (2007) discovered a ~15 K temperature rise near 85 km in the polar region during the January 2005 storm, accompanied by a solar proton event, and attributed this increase to proton precipitation. Nesse Tyssøy et al. (2008) analyzed Na lidar temperature data during the intense geomagnetic storm in January 2005 and found temperatures above 90 km to be higher than the monthly average. They linked these observations to particle precipitation and Joule heating. Zou ZC et al. (2020) conducted a statistical study using observations by the Sounding of the Atmosphere using Broadband Emission Radiometry (SABER) instrument onboard the Thermosphere Ionosphere Mesosphere Energetics and Dynamics (TIMED) satellite. Their results indicated that during intense geomagnetic activity from 2002 to 2018, the temperatures near the mesopause at around 95 km rose by approximately 10 K, with a response delay of up to one day.

In addition, cooling phenomena during storms have been observed in the MLT region in several studies. Pancheva et al. (2007) showed that during the geomagnetic storm at the end of October 2003, the temperature at approximately 90 km showed a significant drop of 25 K, which they attributed to the decrease in ozone. Yuan T et al. (2015) studied four geomagnetic storm events by using Doppler Na lidar and found a substantial increase in temperature above the middle latitude of 95 km. The temperature rise exceeded 55 K above 105 km, and they proposed a close association with the reduction of O/N_2. Lei JH et al. (2011, 2012) reported two geomagnetic storms in October 2003, during which the SABER instrument observed that the NO infrared radiation cooling rate in the lower thermosphere was significantly enhanced, which was an important reason for the decrease in the recovery phase temperature of the storms. This process could even lead to overcooling. Sun M et al. (2022) measured warming exceeding 35 K above 100 km at 80°N during the geomagnetic storm on September 7, 2017, using the SABER instrument on TIMED. They emphasized the role of vertical winds in this warming process. Liu X et al. (2017) used SABER to analyze the geomagnetic storm event in March 2013. They found that the temperature rose by more than 30 K near 80°S at 110 km. They concluded that the global temperature perturbations in the MLT region were caused by changes in global circulation related to Joule heating and ion dragging within the auroral oval. The simulation results of Li JY et al. (2018, 2019) showed that the warming above 105 km during a geomagnetic storm could exceed 30 K at 60°N. Using the thermosphere ionosphere mesosphere electrodynamics general circulation model (TIMEGCM) thermodynamic diagnostic analysis, they demonstrated that mid-latitude temperature changes were mainly caused by adiabatic heating–cooling and vertical convection, both of which were associated with vertical wind perturbations induced by changes in atmospheric circulation.

More recently, research demonstrated that the response of the thermosphere or lower thermosphere to geomagnetic storms exhibited dawn–dusk asymmetry. Zhang YL et al.'s (2022) study of the magnetic storm events from February 3 to 5, 2022, revealed a density increase of 11%–18% on the dusk side at 210 km, whereas on the dawn side, it increased by 18%–26%. They attributed this phenomenon to the prestorm background density on the dawn side and the stronger auroral heating during storm conditions. Li JY et al. (2023), utilizing TIMEGCM, simulated the storm on September 10, 2005. Their results showed that the MLT temperature increased from 12:00 to 24:00 local time (LT) and decreased from 0:00 to 12:00 LT at high latitudes during the early phases of the storm, suggesting that the MLT may exhibit different responses on the dawn side and dusk side during storms. However, their findings lacked observational support.

In this work, we conducted five case studies of extreme magnetic storms and a statistical analysis using SABER observational data to explore the dawn–dusk asymmetry of high-latitude MLT temperature disturbances during the main phase of geomagnetic storms. The organization of this article is as follows: In Section 2, we introduce the SABER instrument and present the list of geomagnetic storms. Section 3 displays the results of case studies for the five extreme magnetic storms. Section 4 provides the statistical results. In Section 5, we continue the discussion on the dawn–dusk asymmetry of temperature disturbances in the high-latitude MLT during the main phase of magnetic storms and investigate the occurrence rates of different temperature disturbances at various altitudes. The conclusions derived from this work are presented in Section 6.

2. Data

The SABER, a scientific instrument mounted on the TIMED satellite, has been operational since January 2002. It continuously measures the profiles of temperature and various trace species within an altitude range of approximately 20 to 110 km. The primary objective of SABER is to provide data on the kinetic temperature, density, infrared radiative rate, and atmospheric composition. These data are crucial for enhancing the understanding of fundamental processes that govern energy, chemistry, dynamics, and transport in the MLT (Russell et al., 1999; Mertens et al., 2003; Remsberg et al., 2003, 2008; Mlynczak et al., 2014). The latitudinal coverage of SABER fluctuates because of the approximately 60-d yaw cycle of the TIMED satellite, spanning from 53°N to 83°S or 83°N to 53°S. The data version used in this paper is V2.0, with a time range from 2002 to 2021 and a height range of 100 to 110 km.

Under the condition in which the minimum disturbance storm time (*Dst*) index value was less than −100 nT and no large geomagnetic storm had occurred on the preceding day of the main phase, a total of 54 geomagnetic storms were filtered from the years 2002 to 2021. The information obtained during the main phase of these geomagnetic storms is shown in Table 1, and the *Dst* index values were derived from the World Data Center for Geomagnetism, Kyoto, Japan (https://wdc.kugi.kyoto-u.ac.jp/).

Table 1. List of main phases of large geomagnetic storms from 2002 to 2021.[a]

Number	Start time (UT)	End time (UT)	Dst_{min} (nT)	Latitude coverage of SABER
1	2002-03-23 15:00	2002-03-24 10:00	−100	83°S to 53°N
2	2002-04-17 12:00	2002-04-20 09:00	−149	83°S to 53°N
3	2002-05-11 11:00	2002-05-11 20:00	−110	83°S to 53°N
4	2002-05-23 12:00	2002-05-23 18:00	−109	53°S to 83°N
5	2002-08-01 11:00	2002-08-02 06:00	−102	83°S to 53°N
6	2002-08-18 21:00	2002-08-21 07:00	−106	83°S to 53°N
7	2002-09-04 02:00	2002-09-04 07:00	−109	83°S to 53°N
8	2002-09-07 13:00	2002-09-08 01:00	−181	83°S to 53°N
9	2002-09-30 22:00	2002-10-01 17:00	−176	53°S to 83°N
10	2002-10-14 03:00	2002-10-14 14:00	−100	53°S to 83°N
11	2002-11-20 17:00	2002-11-21 11:00	−128	53°S to 83°N
12	2003-05-29 13:00	2003-05-29 24:00	−144	53°S to 83°N
13	2003-06-16 07:00	2003-06-18 10:00	−141	53°S to 83°N
14	2003-07-10 18:00	2003-07-12 06:00	−105	53°S to 83°N
15	2003-08-17 15:00	2003-08-18 16:00	−148	83°S to 53°N
16	2003-10-28 08:00	2003-10-30 01:00	−353	53°S to 83°N
17	2003-11-19 23:00	2003-11-20 21:00	−422	53°S to 83°N
18	2004-01-22 04:00	2004-01-22 14:00	−130	53°S to 83°N
19	2004-04-03 15:00	2004-04-04 01:00	−117	83°S to 53°N
20	2004-08-30 01:00	2004-08-30 23:00	−129	83°S to 53°N
21	2004-11-07 13:00	2004-11-08 07:00	−374	53°S to 83°N
22	2005-05-07 20:00	2005-05-08 19:00	−110	83°S to 53°N
23	2005-05-15 04:00	2005-05-15 09:00	−247	83°S to 53°N
24	2005-05-29 23:00	2005-05-30 14:00	−113	53°S to 83°N
25	2005-06-12 18:00	2005-06-13 01:00	−106	53°S to 83°N
26	2005-08-24 07:00	2005-08-24 12:00	−184	83°S to 53°N
27	2005-08-31 13:00	2005-08-31 20:00	−122	83°S to 53°N
28	2005-09-10 14:00	2005-09-11 11:00	−139	83°S to 53°N
29	2006-12-14 15:00	2006-12-15 08:00	−162	83°S to 53°N
30	2011-08-05 20:00	2011-08-06 04:00	−115	83°S to 53°N
31	2011-09-26 14:00	2011-09-26 24:00	−118	53°S to 83°N
32	2011-10-24 19:00	2011-10-25 02:00	−147	53°S to 83°N
33	2012-04-23 17:00	2012-04-24 05:00	−120	83°S to 53°N
34	2012-07-15 01:00	2012-07-15 19:00	−139	83°S to 53°N
35	2012-09-30 14:00	2012-10-01 05:00	−122	53°S to 83°N
36	2012-10-07 13:00	2012-10-09 09:00	−109	53°S to 83°N
37	2012-11-13 18:00	2012-11-14 08:00	−108	53°S to 83°N
38	2013-03-17 07:00	2013-03-17 21:00	−132	83°S to 53°N
39	2013-06-01 01:00	2013-06-01 09:00	−124	53°S to 83°N
40	2013-06-28 01:00	2013-06-29 02:00	−100	53°S to 83°N
41	2014-02-18 14:00	2014-02-19 09:00	−119	53°S to 83°N
42	2015-01-07 08:00	2015-01-07 12:00	−107	53°S to 83°N
43	2015-03-17 06:00	2015-03-17 23:00	−234	83°S to 53°N

Continued from Table 1

Number	Start time (UT)	End time (UT)	Dst_{min} (nT)	Latitude coverage of SABER
44	2015-06-22 12:00	2015-06-23 05:00	−198	53°S to 83°N
45	2015-08-25 23:00	2015-08-27 21:00	−103	83°S to 53°N
46	2015-10-07 03:00	2015-10-07 23:00	−130	53°S to 83°N
47	2015-12-20 04:00	2015-12-20 23:00	−166	83°S to 53°N
48	2015-12-31 12:00	2016-01-01 01:00	−116	83°S to 53°N
49	2016-01-20 02:00	2016-01-20 17:00	−101	53°S to 83°N
50	2016-10-13 03:00	2016-10-13 18:00	−110	53°S to 83°N
51	2017-05-27 22:00	2017-05-28 08:00	−125	53°S to 83°N
52	2017-09-07 20:00	2017-09-08 02:00	−122	53°S to 83°N
53	2018-08-25 14:00	2018-08-26 07:00	−175	83°S to 53°N
54	2021-11-03 21:00	2021-11-03 14:00	−105	83°S to 53°N

[a]The regions referred to as dawn side and dusk side in this article correspond to the time ranges of 03:00–09:00 LT and 15:00–21:00 LT, respectively.

3. The MLT Temperature Response during Geomagnetic Superstorms

In this study, an analysis was initially conducted on five geomagnetic superstorm events, which were selected based on their minimum *Dst* values being lower than −200 nT during the period from 2002 to 2021. The chosen events occurred on October 27–31, 2003; November 19–20, 2003; November 7–8, 2004; May 15, 2005; and March 17, 2015. In Figure 1a, the *Dst* index for October 27–31, 2003, is presented, highlighting the first main phase of the geomagnetic storm in the yellow-shaded region. The *Dst* value began decreasing from 07:00 universal time (UT) on October 29, reached a minimum of −151 nT at 11:00 UT, began recovering, resumed descending at 14:00 UT, and concluded at −353 nT by 01:00 UT on October 30, followed by the recovery phase. In this event, SABER observations covered latitudes from 52°S to 83°N. Consequently, temperature observations were filtered for altitudes between 100 and 110 km and latitudes above 60°N from October 27 to 31. The temperature profiles averaged over 7:00 UT on October 27 to 7:00 UT on October 29, corresponding to the 48 h preceding the main phase of the geomagnetic storm, were selected as the reference temperatures during quiet periods. The temperature profiles from October 27 to 31 were then subtracted from the reference profiles. To eliminate diurnal and semidiurnal variations, a zonal running mean was applied with a window width of 24 h. The resulting plot in Figure 1b illustrates the variations in high-latitude MLT temperatures during the event. Although the results do not precisely quantify the temperature disturbance in the region, they reflect the overall trend of temperature disturbances. The black dashed line in Figure 1b marks the start and end times of the main phase of the geomagnetic storm corresponding to Figure 1a. Figure 1b reveals that the warming during this event began around 16:00 UT on October 28, preceding the main phase, which was attributed to the zonal running mean operation and weak geomagnetic activity before the main phase. Subsequently, the temperature reached its maximum value around 05:00 UT on October 30, with a warming of nearly 60 K at 110 km. This warming propagated downward from higher altitudes to below 100 km, reaching approximately 15 K at 100 km. Following this, a secondary geomagnetic storm occurred, with a minimum *Dst* value reaching −383 nT, during which no significant increase in temperature occurred at higher altitudes. Figure 1c illustrates the temperature disturbance intervals corresponding to observation points during the main phase of this event, with a statistical height range of 100–110 km. The median temperature disturbance was 22.4 K, with a minimum of −54.4 K. We found that 2.4% of disturbances exceeded 100 K, and only 21.7% of the observation points had temperature disturbances below 0 K. Figure 1d illustrates the local times corresponding to the high-latitude observation points during the main phase. In this event, 56.0% of the observation points were between 12:00 and 24:00 LT, 47.3% were between 15:00 and 21:00 LT, and no points were between 03:00 and 09:00 LT, indicating the prevalence of observations on the dusk side.

Figure 2, similar to Figure 1, corresponds to the geomagnetic storm event that occurred from November 19 to 20, 2003. The main phase of this event commenced at 23:00 UT on November 19, with a *Dst* value of −2 nT, and concluded at 22:00 UT on November 20, reaching a minimum *Dst* value of −422 nT. In Figure 2b, the quiet period selected for baseline temperature comparison spans from 23:00 UT on November 17 to 23:00 UT on November 19, covering latitudes above 60°N. It can be observed that during the main phase, temperatures continuously increased above 105 km, exceeding 60 K at 110 km around 02:00 UT on November 21. Additionally, temperatures below 105 km initially increased, then decreased, and experienced another rise around 15:00 UT, with warming reaching up to 10 K near 100 km. Figure 2c demonstrates that for the majority of observation points during this event, temperature disturbances were positive. From the statistical results, the median temperature disturbance was 18.3 K, with negative disturbances accounting for only 25.9%. The minimum disturbance was −59.4 K, and 3.2% of the observation points had temperature disturbances exceeding 100 K. Additionally, all observation points during this event were between 12:00 and 24:00 LT, with 23.9% recorded between 15:00 and 21:00 LT.

Figure 3 presents the analysis of the geomagnetic storm event

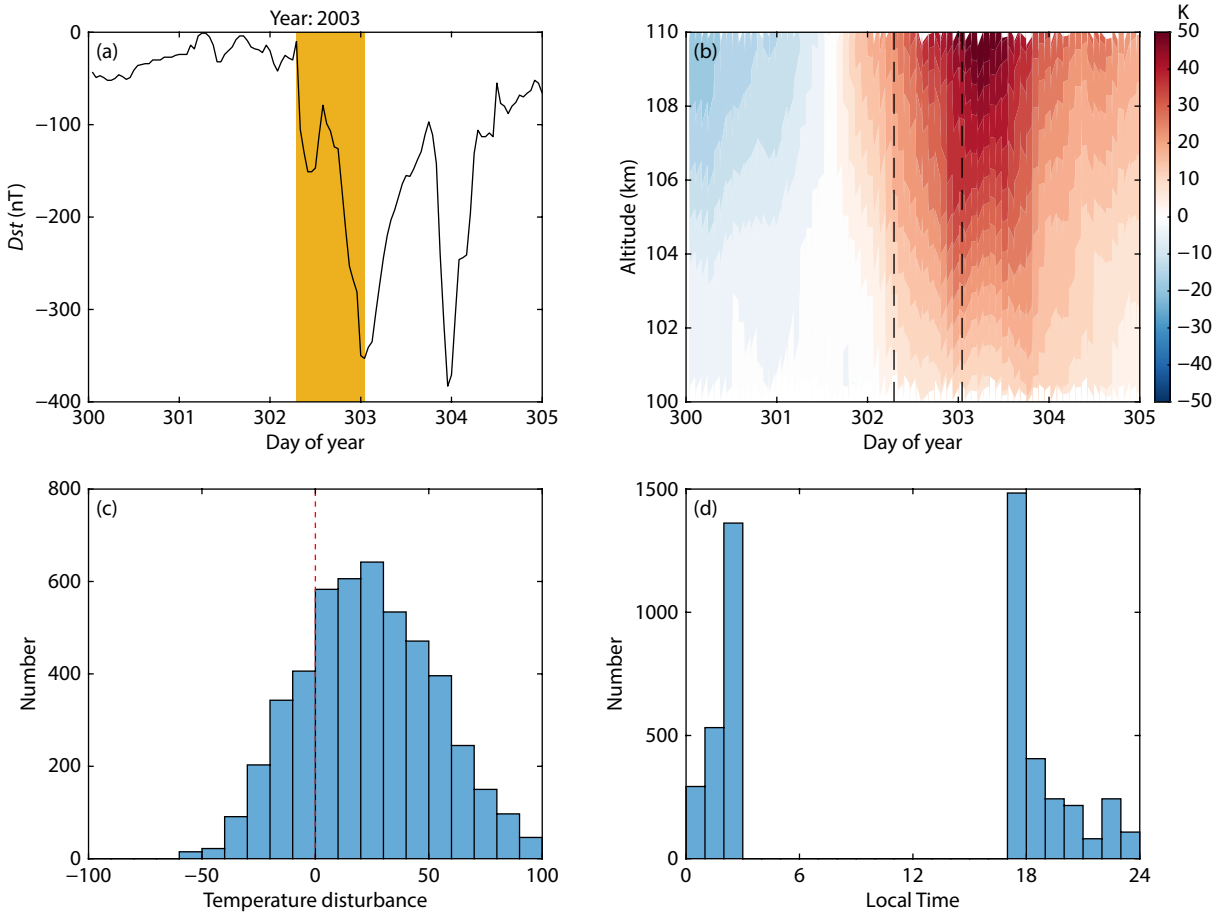

Figure 1. (a) October 27–31, 2003, *Dst* index, with the yellow-shaded region indicating the first-phase main phase of the geomagnetic storm event. (b) Temperature variations in the MLT region above 60°N and between 100 and 110 km. The average temperature profiles during the 48 h preceding the main phase of the geomagnetic storm, from 7:00 UT on October 27 to 7:00 UT on October 29, were subtracted from the temperature profiles during the storm period from October 27 to 31. A 24-h zonal running mean was applied for smoothing. The black dashed line in the figure marks the onset and end times of the geomagnetic storm main phase corresponding to (a). (c) The statistical results of temperature disturbance intervals (at a statistical height range of 100–110 km) corresponding to observation points during the first main phase of this event. (d) Local times corresponding to the high-latitude observation points during the main phase of the event.

that took place from November 7 to 8, 2004. The main phase of this event began at 13:00 UT on November 7, reaching the minimum *Dst* value of −15 nT at 18:00 UT. Subsequently, the *Dst* value began to rise, reaching 61 nT at 20:00 UT before descending again, and concluded at 07:00 UT on November 8, corresponding to a minimum *Dst* value of −374 nT. During this event, temperatures above 60°N showed a sharp increase over time, with a warming of nearly 80 K observed at 110 km altitude at the end of the main phase, and a peak near 100 K around 19:00 UT on November 8. The statistical results for the observation points indicated that the temperature variations within the 100–110 km range during the main phase were primarily characterized by heating. Specifically, the minimum temperature disturbance was −71.4 K, the median was 12.3 K, and 1.0% of the observation points had temperature disturbances exceeding 100 K. As shown in Figure 3d, 72.7% of the observation points fell within the time range of 12:00 to 24:00 LT, and 55.1% of the total were recorded between 15:00 and 21:00 LT. In other words, more than half of the observation points were located on the dusk side.

The fourth event with a minimum *Dst* value below −200 nT had a relatively short duration, lasting only 5 h during the main phase from 04:00 UT to 09:00 UT on May 15, 2005, with a minimum *Dst* value of −247 nT. This is reflected in Figure 4b as a weaker warming. In this event, temperatures in the MLT region at latitudes of 60°S and above showed a gradual increase during the main phase of the storm, with the temperature disturbance sliding window average over a 24-h window being less than 60 K. Similar to the geomagnetic storm event in November 2003, in this event, 33.0% of the observation points had temperature disturbances less than 0 K, whereas those exceeding 100 K constituted 0.2%. The disturbance median was 8.6 K, and all observation points were between 12:00 and 24:00 LT, with 26.9% falling between 15:00 and 21:00 LT.

Figure 5 corresponds to the geomagnetic storm event on March 17, 2015, with the main phase occurring from 6:00 to 23:00 UT, and a minimum *Dst* value of −234 nT. Figure 5b illustrates that unlike the previous four events, the temperature changes during the main phase were primarily characterized by cooling, with a minimum decrease of 7 K. Additionally, the warming during the recovery phase was not prominent, with a maximum increase of

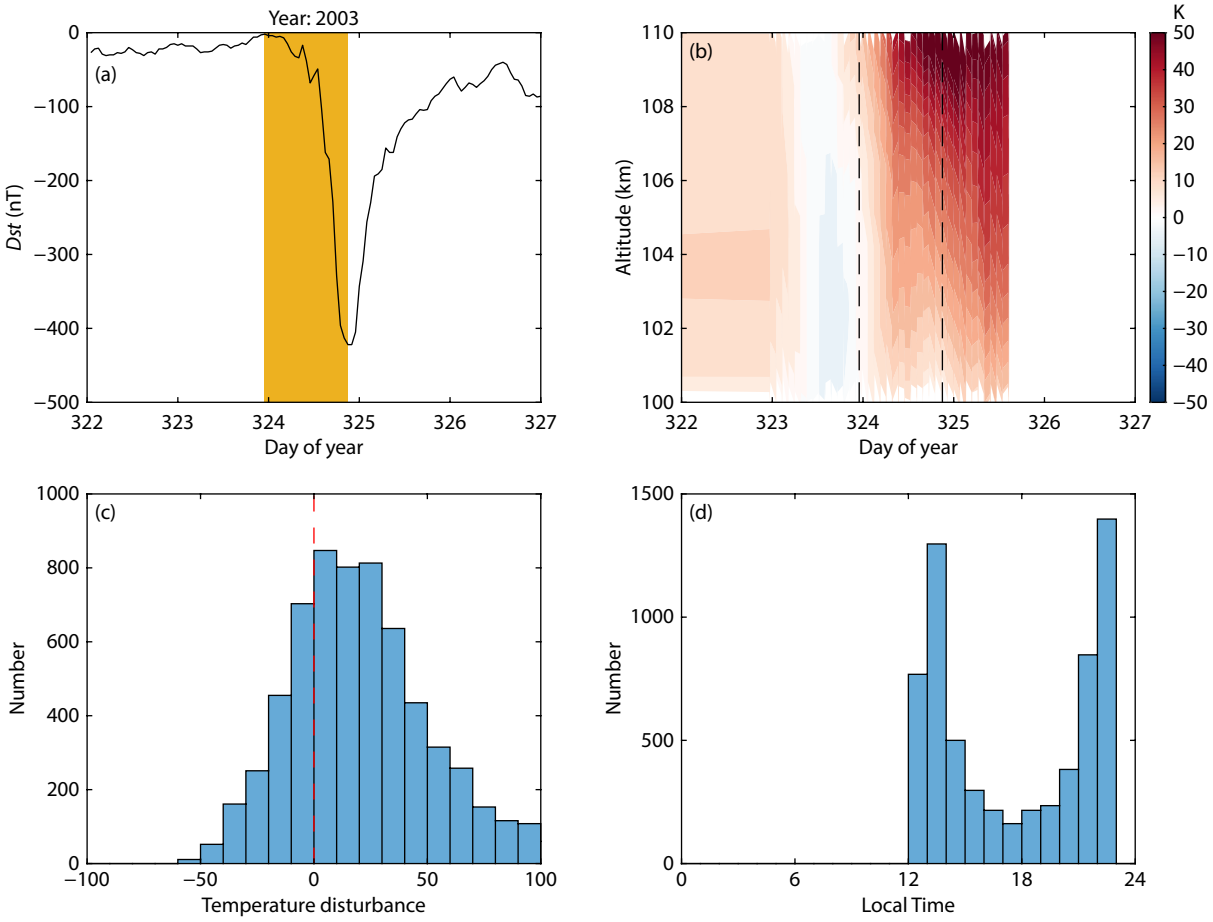

Figure 2. Similar to Figure 1 but corresponding to the geomagnetic storm event from November 19 to 20, 2003.

25 K at 110 km. Furthermore, the observation points during this event were mainly distributed between 00:00 and 12:00 LT (Figure 5d), with points between 3:00 and 9:00 LT accounting for 39.1% of the total. During the main phase of this event, a significant amount of cooling was observed, constituting 56.4% of the total observation points, exceeding half of the dataset. We observed few instances of noticeable warming, with the minimum temperature disturbance being −62.8 K and a disturbance median of −3.1 K. Warming exceeding 50 K accounted for only 1.4%, as depicted in Figure 5c.

According to the analysis of the five extreme magnetic storms during the period from 2002 to 2021, we observed that the high-latitude MLT observation points during the main phase of the storms in the first four events were predominantly located on the dusk side and that temperatures increased during the main phase. In contrast, the event in March 2015, in which the observation points were mainly situated on the dawn side, exhibited significant cooling during the main phase. Compared with the event in May 2005, the March 2015 event showed a notably higher rate of cooling despite having a similar minimum *Dst* value and a longer duration. Therefore, we can infer an asymmetry in temperature changes on the dawn and dusk sides of the high-latitude MLT during the main phase of magnetic storms. Specifically, a tendency exists for more cooling on the dawn side and more warming on the dusk side. In addition, it is worth noting that the Dst_{min} values corresponding to the main phase of geomagnetic storm events in Figures 1–5, within the 48 h before the main phase, were −52, −36, −3, −42, and −11 nT, respectively. This result implies that weak geomagnetic disturbances were present before the main phase of the geomagnetic storm events on October 28, 2003 (Figure 1), November 19, 2003 (Figure 2), and May 15, 2005 (Figure 4). The observation points of SABER during these events were mainly located on the dusk side, where early geomagnetic activity would heat up the region through weak dynamic and Joule heating processes, causing the actual temperature during quiet periods to be slightly lower than the calculated temperature mean. Taking Figure 1 as an example, this resulted in a relatively underestimated temperature perturbation value, indicating that the real distribution in Figure 1c tended to be biased toward the warming side, consistent with the conclusion of higher temperatures on the dusk side.

4. Statistical Results

To further substantiate this conclusion, temperature observation data during the main phase of the 54 events (as listed in Table 1) were selected. These events were confined to latitudes above 60° and altitudes within the 100–110 km range. The data were categorized by local time, with temperatures from 03:00 to 09:00 LT (dawn side) subtracted from the average temperatures of the quiet period (48 h before the main phase) for the dawn side. Simi-

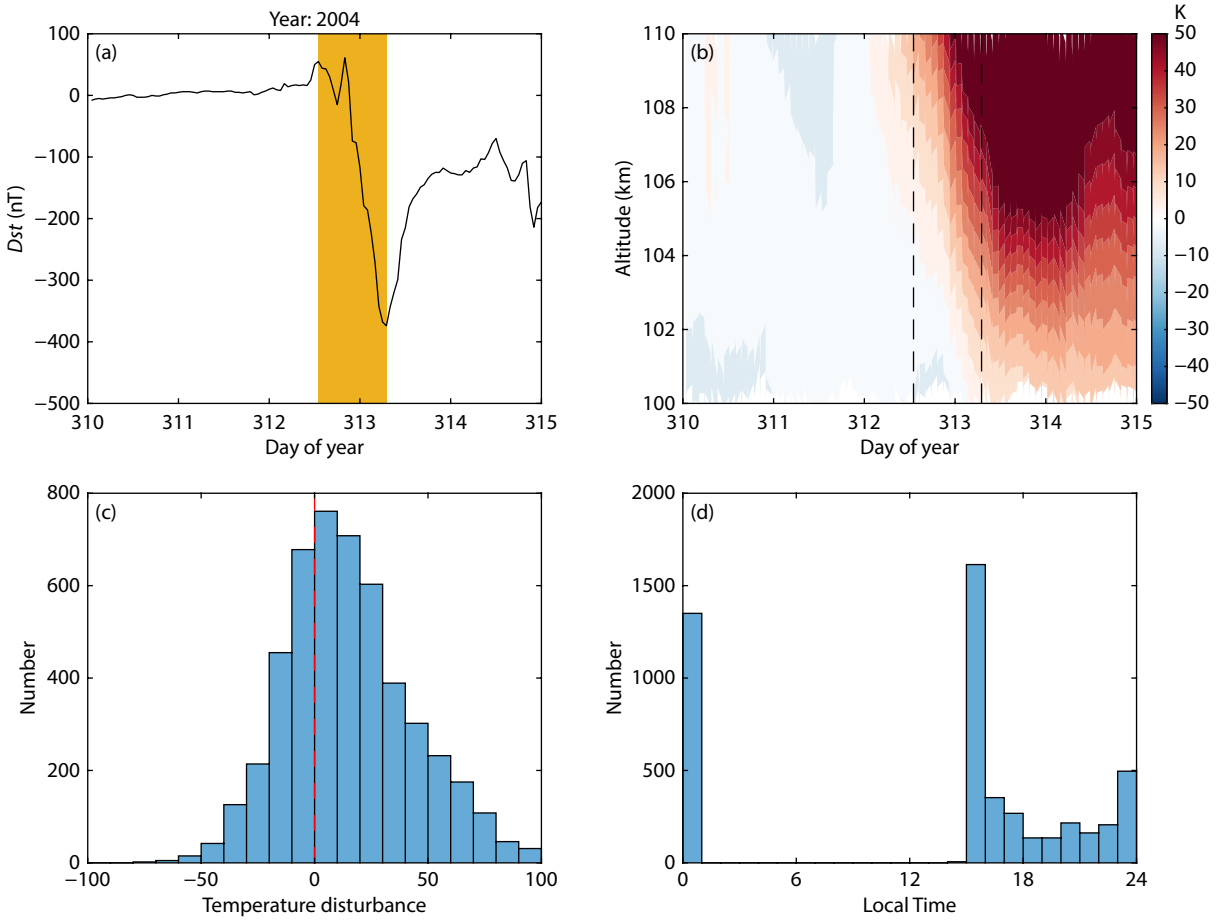

Figure 3. Similar to Figure 1 but corresponding to the geomagnetic storm event from November 7 to 8, 2004.

larly, temperatures from 15:00 to 21:00 LT (dusk side) were subtracted from the dusk side quiet period (48 h before the onset of the main phase). In this way, temperature disturbances corresponding to latitudes above 60° on the dawn side (dusk side) within the altitude range of 100–110 km were obtained for each observation point. Subsequently, on the basis of the temperature disturbances, the observation points on the dawn side (dusk side) were allocated to different disturbance intervals, in intervals of 10 K. The quantity within each interval was then normalized by calculating the probabilities of various temperature disturbances occurring, as shown in Figure 6a. In this figure, the red line represents the frequency of different temperature disturbances on the dusk side, the blue line indicates that for the dawn side, and the black line indicates the difference between the dusk and dawn sides. The results indicate that the occurrence of 0 K disturbances was the highest on the dawn side, accounting for approximately 13.7%. This proportion decreased with an increase in the absolute value of the disturbance magnitude. Points with cooling exceeding −5 K constituted 38.2% of the total, whereas points with warming exceeding 100 K accounted for only 2.0%. In contrast, on the dusk side, the occurrence rate of temperature disturbances peaked around 10 K, with a proportion of 12.1%. Points with cooling exceeding −5 K represented 29.5% of the total, and a higher proportion was observed for intense disturbances, with points showing warming of 100 K or more accounting for 4.3% of the total. However, the occurrence rates of temperature disturbances below 10 K were relatively less frequent in this category. Figure 6c presents the ratio of the occurrence rates of different temperature disturbances between the dawn and dusk sides. The blue color corresponds to the ratio of dawn to dusk, and the red color corresponds to the ratio of dusk to dawn. The frequency of −90 K disturbances was significantly higher on the dawn side, approximately 2.53 times higher than that on the dusk side. This ratio generally decreased with a decreasing disturbance magnitude, reaching 1.05 at 20 K. When disturbances were greater than 20 K, the frequency on the dusk side began to exceed that on the dawn side, with the ratio increasing with the magnitude of the disturbance, reaching 2.16 at 90 K.

As a comparison, Figure 6b illustrates the occurrence rates of temperature disturbances for the latitudinal range of 30° to 60°. In the mid-latitudes, both the dawn and dusk sides exhibited the maximum occurrence rates of temperature disturbances near 0 K, reaching 15.6% and 13.9%, respectively. Relative to high latitudes, temperature disturbances in the mid-latitudes were weaker. It is noteworthy that the dawn–dusk asymmetry in the mid-latitudes exhibited differences from those at high latitudes. The occurrence rates of perturbations exceeding 30 K on the dusk side (including both positive and negative perturbations) were consistently higher than those on the dawn side. This result implies that, overall, temperature perturbations on the dusk side in the mid-latitudes were stronger than those on the dawn side.

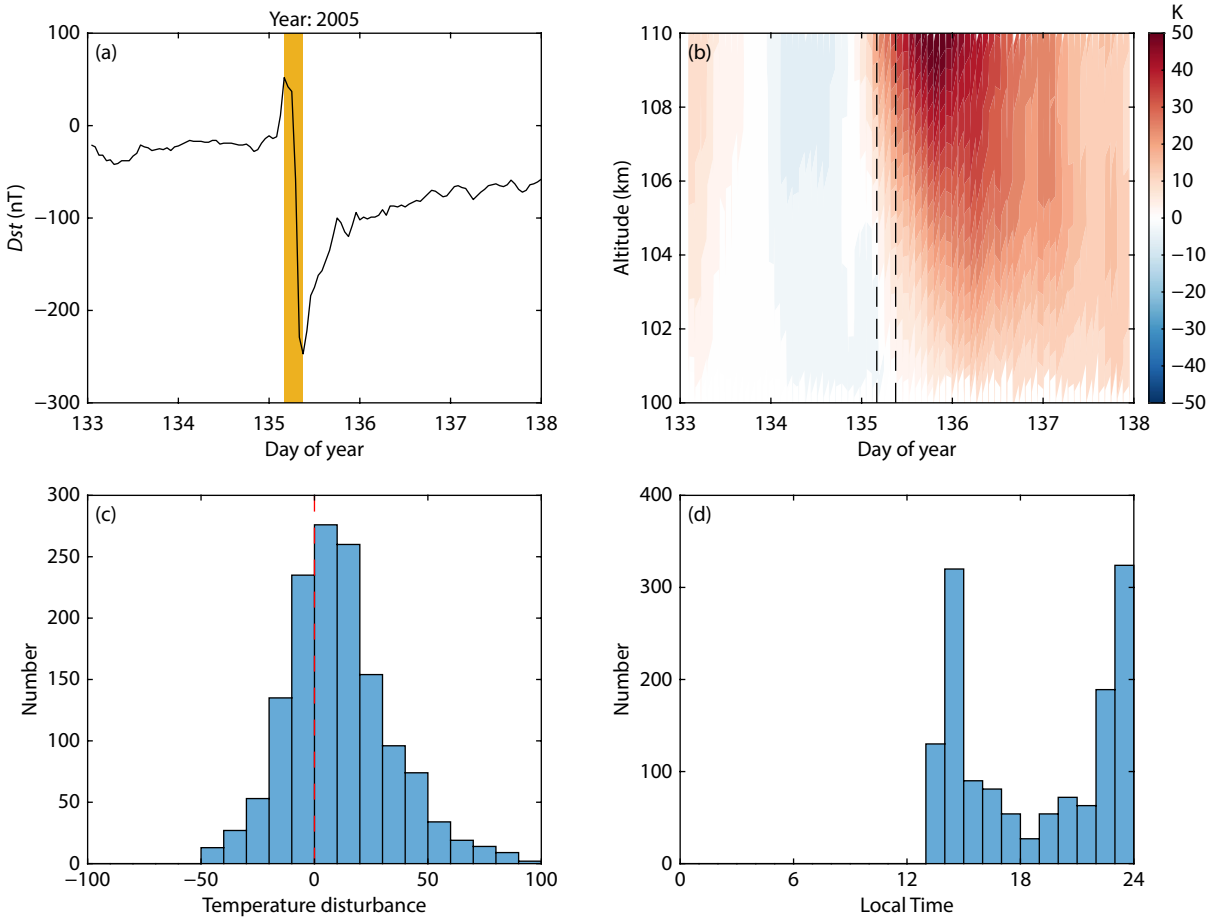

Figure 4. Similar to Figure 1 but corresponding to the geomagnetic storm event on May 15, 2005.

5. Discussion

The conclusions regarding the dawn–dusk asymmetry in high-latitude MLT temperature disturbances during the main phase of geomagnetic storms, as presented in Figures 1 to 6, can be explained by the simulation conducted by Li JY et al. (2023). During the main phase of geomagnetic storms, the MLT region on the night side, particularly in the auroral oval and polar cap regions, experiences upward vertical wind perturbations induced by the upper level vertical wind. This leads to adiabatic expansion and vertical convection, both contributing to cooling processes. Although processes such as Joule heating may weaken these cooling mechanisms, the heating mechanism at these altitudes during high-latitude storms, induced by the vertical wind, dominates these two processes. As a result, the total heating rate on the high-latitude night side becomes negative. This cooling process extends to the dawn side, significantly influencing the final temperature, which is lower than the prestorm level. Furthermore, around the latitude of 60° on the dawn side, certain upward vertical wind perturbations occur during the main phase of geomagnetic storms, contributing to the observed cooling phenomenon. However, Figure 6a reveals that during the main phase of geomagnetic storms, the occurrence rate of negative temperature disturbances on the dawn side of the high-latitude MLT is 36.4%, which is less than the occurrence rate of positive disturbances (50.4%). This result may suggest that the simulated cooling induced by the vertical wind is relatively larger than the actual values.

In contrast to the dawn side, during the main phase of geomagnetic storms on the day side, the high-latitude MLT region experiences downward vertical wind perturbations. Although the intensity of these perturbations is weaker than the upward vertical wind perturbations on the night side, the associated adiabatic compression and vertical convective processes still have a certain impact on the total heating on the day side. Simultaneously, Joule heating plays a crucial role in warming the high-latitude MLT region on the day side during storm times. The heating induced by Joule heating, combined with the heating caused by the vertical wind, results in a significant overall heating on the day side at high latitudes. Consequently, the temperatures on the dusk side generally increase, leading to a higher proportion of positive temperature disturbances than negative disturbances on the dusk side, as observed in Figure 6a.

To illustrate the relationship between high-latitude MLT temperature disturbances and altitude during the main phase of geomagnetic storms, Figure 7 presents the occurrence rates of temperature disturbances in the range of −90 to 90 K at different altitudes for the 54 storm events. In the case of latitudes above 60°, as shown in Figure 7a, the distribution of warming exceeding 50 K exhibits an increasing trend with altitude. This increase is attributed to the greater influence of processes such as Joule heating, vertical convection, and adiabatic compression at higher altitudes. Under

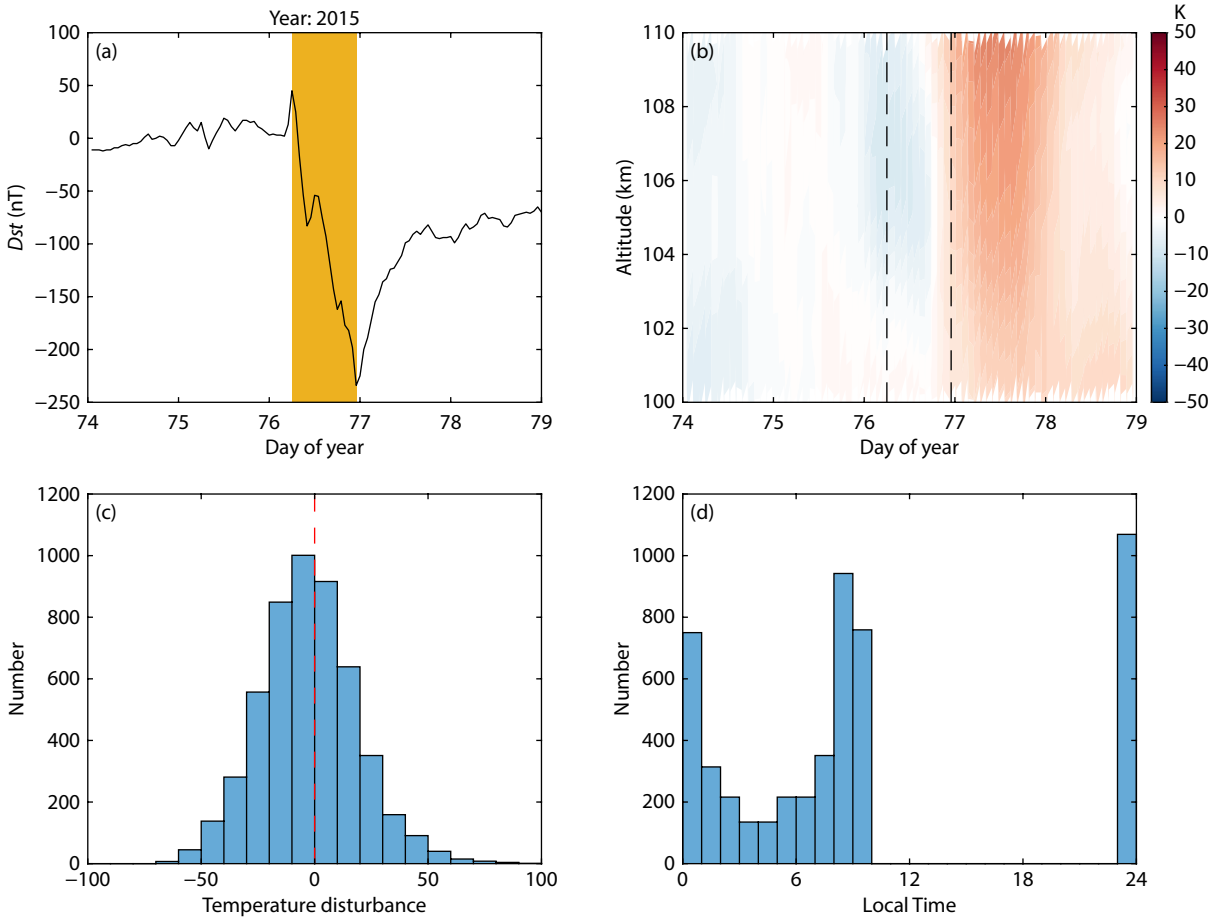

Figure 5. Similar to Figure 1 but corresponding to the geomagnetic storm event on March 17, 2015.

the condition of weak temperature disturbances within the range of −30 to 30 K, the occurrence rate decreases with increasing altitude. In contrast to warming situations, cooling below −50 K is more prevalent at lower altitudes. Additionally, as the negative disturbances intensify, the occurrence rate near 110 km decreases, possibly because of stronger Joule heating at higher altitudes at high latitudes resulting in fewer cooling phenomena. Figures 7c and 7e are similar to Figure 7a but correspond to the dawn and dusk sides, respectively. They do not show significant differences. However, the main difference lies in the concentration of strong temperature disturbances below −90 K on the dusk side, centered around 104 to 106 km, accounting for 39.6%. On the dawn side, a significant proportion of strong cooling also occurs near 100 km.

Figure 7b illustrates the occurrence rates of temperature disturbances in the mid-latitude MLT during the main phase of geomagnetic storms at different altitudes. The occurrence rates in the mid-latitudes for weak disturbances and strong warming are similar to those at high latitudes (Figure 7a). However, in contrast to high latitudes, the occurrence rates of strong cooling during storm times on the mid-latitude day side increase with altitude in the MLT region, similar to the warming pattern. This observation is consistent with the findings of Li JY et al. (2018), where the dominant mechanisms governing MLT temperature disturbances in the mid-latitudes during storms are adiabatic heating–cooling and vertical thermal convection. The overall effects decrease with decreasing altitude, leading to a reduction in the occurrence rates of strong temperature disturbances with decreasing altitude. Furthermore, Figures 7d and 7f indicate no apparent dawn–dusk asymmetry in the relationship between the occurrence rates of temperature disturbances and altitude in the mid-latitudes, just as at the high latitudes.

6. Summary

In this work, we investigated the differences in temperature disturbances in the high-latitude MLT region between the dawn and dusk sides during the main phase of five extreme geomagnetic storms. The main conclusions are summarized as follows:

(1) Among the five extreme geomagnetic storms occurring between 2002 and 2021, the storm event in March 2015 exhibited the predominant presence of high-latitude observation points on the dawn side. The observed temperature disturbances during this event generally skewed toward negative values, with 56.4% of the observations having disturbances less than 0 K. In contrast, the observation points during the main phase of the preceding four events were predominantly on the dusk side, and the temperature disturbances were mostly warming, with the proportions of disturbances less than 0 K ranging from 21.7% to 33.0%.

(2) Among the 54 large geomagnetic storm events during 2002–2021, the occurrence of cooling in the high-latitude MLT region during the main phase was more prominent on the dawn side than the dusk side. The occurrence rates of cooling exceeding

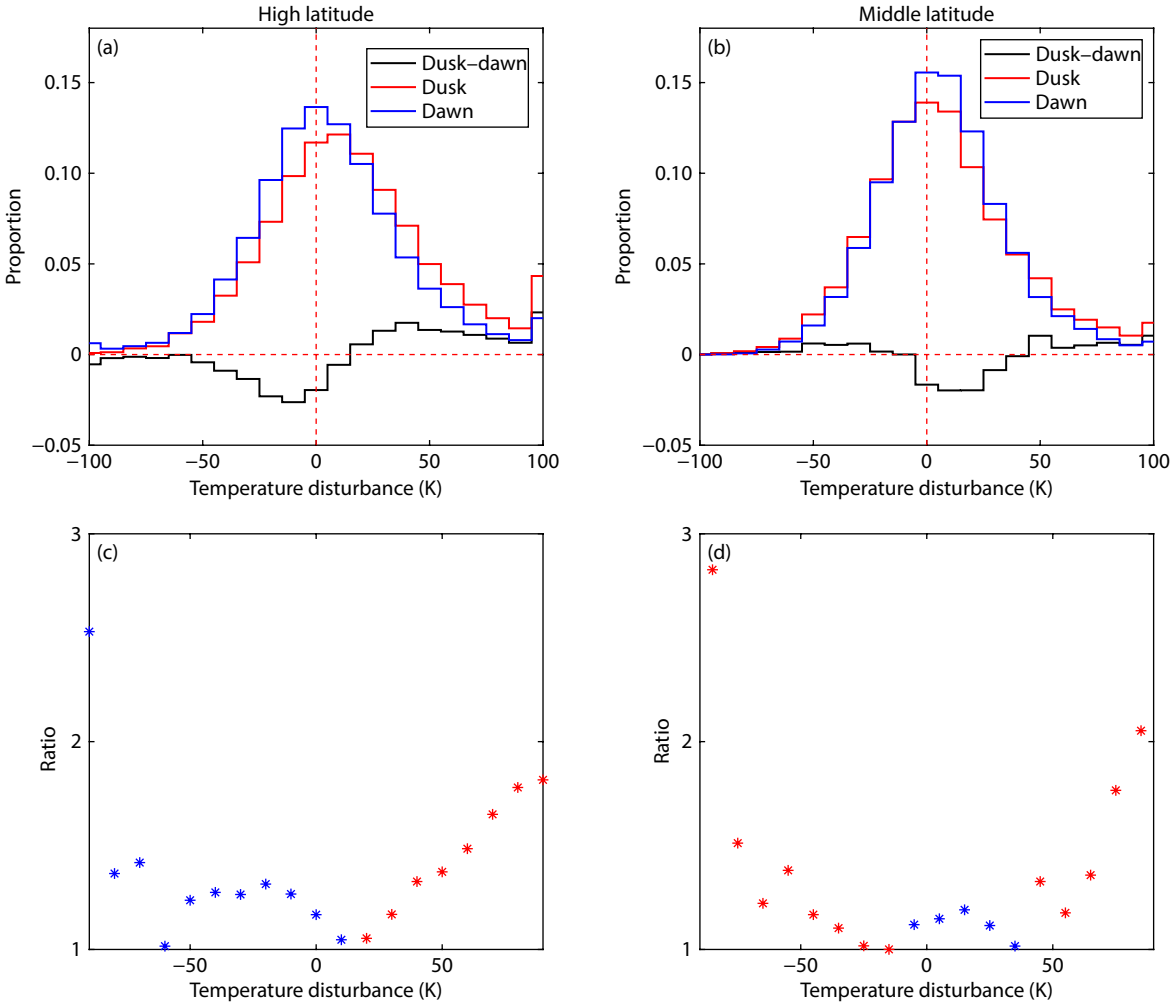

Figure 6. (a) The normalized count of observation points in different temperature disturbance intervals on the dawn and dusk sides, with intervals spanning 10 K. The data were sourced from temperature observations during the main phases of all 54 events at latitudes above 60° and within the range of 100–110 km. The red line represents the occurrence rate of different temperature disturbances on the dusk side, the blue line represents those on the dawn side, and the black line illustrates the difference between those on the dusk and dawn sides. (b) Similar to (a) but corresponding to the mid-latitudes of 30° to 60°. (c) Ratio of occurrence rates of temperature disturbances on the dawn side to the dusk side at different disturbance intervals (larger values compared with smaller values). Blue indicates a higher occurrence rate on the dawn side within the same interval, whereas red indicates a higher occurrence rate on the dusk side. (d) Similar to (c) but corresponding to the mid-latitudes.

−5 K were 38.2% on the dawn side and 29.5% on the dusk side.

(3) The intense warming on the dawn side was weaker compared with that on the dusk side, with occurrence rates of warming exceeding 100 K being 2.0% on the dawn side and 4.3% on the dusk side.

(4) The occurrence rates of temperature disturbances on both the dawn and dusk sides during the main phase of high-latitude MLT warming increased with altitude. Cooling occurrence rates were smaller above 108 km, and on the dusk side, cooling was mainly concentrated near 105 km.

(5) The mid-latitudes did not exhibit significant dawn–dusk asymmetry, and both cooling and warming occurrence rates increased with altitude.

Acknowledgments

This work was supported by the National Key R&D Program of China (Grant No. 2022YFF0503702), the National Natural Science Foundation of China (Grant Nos. 42004132, 42074195 and 42074183), the open funding of the Ministry of Natural Resources Key Laboratory for Polar Science (Grant No. KP202104), and the China Geological Survey (Grant No. ZD20220145).

References

Banks, P. M. (1979). Joule heating in the high-latitude mesosphere. *J. Geophys. Res.: Space Phys.*, *84*(A11), 6709–6712. https://doi.org/10.1029/JA084iA11p06709

Fagundes, P. R., Sahai, Y., Takahashi, H., Gobbi, D., and Bittencourt, J. A. (1996). Thermospheric and mesospheric temperatures during geomagnetic storms at 23°S. *J. Atmos. Terr. Phys.*, *58*(16), 1963–1972. https://doi.org/10.1016/0021-9169(96)00001-3

Fejer, B. G., Blanc, M., and Richmond, A. D. (2017). Post-storm middle and low-latitude ionospheric electric fields effects. *Space Sci. Rev.*, *206*(1-4), 407–429. https://doi.org/10.1007/s11214-016-0320-x

Lei, J. H., Thayer, J. P., Lu, G., Burns, A. G., Wang, W. B., Sutton, E. K., and Emery, B. A. (2011). Rapid recovery of thermosphere density during the October 2003

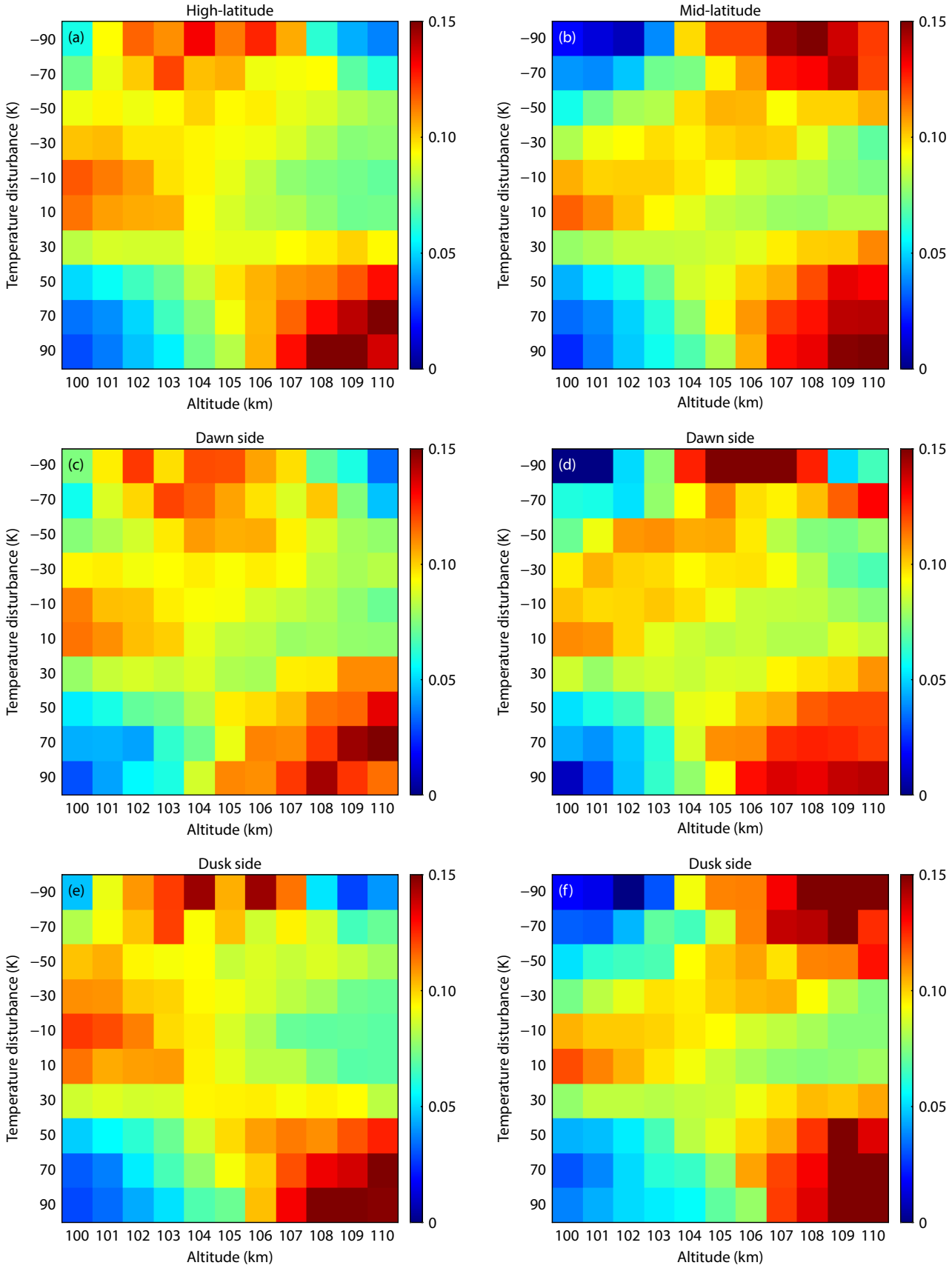

Figure 7. (a) The occurrence rates of temperature disturbances in the range of −90 to 90 K at different altitudes during 54 geomagnetic storm events at high latitudes (above 60°). (b) Similar to (a) but corresponding to mid-latitudes in the range of 30° to 60°. (c–f) The dawn side (3:00 to 9:00 LT) at high latitudes, the dawn side at mid-latitudes, the dusk side (15:00 to 21:00 LT) at high latitudes, and the dusk side at mid-latitudes, respectively.

geomagnetic storms. *J. Geophys. Res.: Space Phys.*, *116*(A3), A03306. https://doi.org/10.1029/2010JA016164

Lei, J. H., Burns, A. G., Thayer, J. P., Wang, W. B., Mlynczak, M. G., Hunt, L. A., Dou, X. K., and Sutton, E. (2012). Overcooling in the upper thermosphere during the recovery phase of the 2003 October storms. *J. Geophys. Res.: Space Phys.*, *117*(A3), A03314. https://doi.org/10.1029/2011JA016994

Li, J. Y., Wang, W. B., Lu, J. Y., Yuan, T., Yue, J., Liu, X., Zhang, K. D., Burns, A. G., Zhang, Y. L., and Li, Z. (2018). On the responses of mesosphere and lower thermosphere temperatures to geomagnetic storms at low and middle latitudes. *Geophys. Res. Lett.*, *45*(19), 10128–10137. https://doi.org/10.1029/2018GL078968

Li, J. Y., Wang, W. B., Lu, J. Y., Yue, J., Burns, A. G., Yuan, T., Chen, X. T., and Dong, W. J. (2019). A modeling study of the responses of mesosphere and lower thermosphere winds to geomagnetic storms at middle latitudes. *J. Geophys. Res.: Space. Phys.*, *124*(5), 3666–3680. https://doi.org/10.1029/2019JA026533

Li, J. Y., Wei, G. C., Wang, W. B., Luo, Q. S., Lu, J. Y., Tian, Y. F., Xiong, S. P., Sun, M., Shen, F. Z., … Yang, C. L. (2023). A modeling study on the responses of the mesosphere and lower thermosphere (MLT) temperature to the initial and main phases of geomagnetic storms at high latitudes. *J. Geophys. Res.: Atmos.*, *128*(10), e2022JD038348. https://doi.org/10.1029/2022JD038348

Liu, X., Yue, J., Xu, J. Y., Garcia, R. R., Russell III, J. M., Mlynczak, M., Wu, D. L., and Nakamura, T. (2017). Variations of global gravity waves derived from 14 years of SABER temperature observations. *J. Geophys. Res.: Atmos.*, *122*(12), 6231–6249. https://doi.org/10.1002/2017JD026604

Mertens, C. J., Mlynczak, M. G., Lopez-Puertas, M., Wintersteiner, P. P., Picard, R. H., Winick, J. R., Gordley, L. L., and Russell III, J. M., (2003). Retrieval of kinetic temperature and carbon dioxide abundance from nonlocal thermodynamic equilibrium limb emission measurements made by the SABER experiment on the TIMED satellite. In *Proceedings of SPIE 4882, Remote Sensing of Clouds and the Atmosphere VII* (pp. 162–171). Crete, Greece: SPIE. https://doi.org/10.1117/12.463358

Mlynczak, M. G., Hunt, L. A., Mertens, C. J., Marshall, B. T., Russell III, J. M., Woods, T., Thompson, R. E., and Gordley, L. L. (2014). Influence of solar variability on the infrared radiative cooling of the thermosphere from 2002 to 2014. *Geophys. Res. Lett.*, *41*(7), 2508–2513. https://doi.org/10.1002/2014GL059556

Nesse Tyssøy, H., Heinrich, D., Stadsnes, J., Sørbø, M., Hoppe, U. P., Evans, D. S., Williams, B. P., and Honary, F. (2008). Upper-mesospheric temperatures measured during intense substorms in the declining phase of the January 2005 solar proton events. *Ann. Geophys.*, *26*(9), 2515–2529. https://doi.org/10.5194/angeo-26-2515-2008

Pancheva, D., Singer, W., and Mukhtarov, P. (2007). Regional response of the mesosphere-lower thermosphere dynamics over Scandinavia to solar proton events and geomagnetic storms in late October 2003. *J. Atmos. Sol. Terr. Phys.*, *69*(9), 1075–1094. https://doi.org/10.1016/j.jastp.2007.04.005

Remsberg, E., Lingenfelser, G., Harvey, V. L., Grose, W., Russell, J., Mlynczak, M., Gordley, L., and Marshall, B. T. (2003). On the verification of the quality of SABER temperature, geopotential height, and wind fields by comparison with Met Office assimilated analyses. *J. Geophys. Res.: Atmos.*, *108*(D20), 4628. https://doi.org/10.1029/2003JD003720

Remsberg, E. E., Marshall, B. T., Garcia-Comas, M., Krueger, D., Lingenfelser, G. S., Martin-Torres, J., Mlynczak, M. G., Russell III, J. M., Smith, A. K., … Thompson, R. E. (2008). Assessment of the quality of the Version 1.07 temperature-versus-pressure profiles of the middle atmosphere from TIMED/SABER. *J. Geophys. Res.: Atmos.*, *113*(D17), D17101. https://doi.org/10.1029/2008JD010013

Roble, R. G., Emery, B. A., Killeen, T. L., Reid, G. C., Solomon, S., Garcia, R. R., Evans, D. S., Hays, P. B., Carignan, G. R., … Brace, L. H. (1987). Joule heating in the mesosphere and thermosphere during the July 13, 1982, solar proton event. *J. Geophys. Res.: Space Phys.*, *92*(A6), 6083–6090. https://doi.org/10.1029/ja092ia06p06083

Russell III, J. M., Mlynczak, M. G., Gordley, L. L., Tansock, J. J., Jr., and Esplin, R. W. (1999). Overview of the SABER experiment and preliminary calibration results. In *Proceedings of SPIE* 3756, *Optical Spectroscopic Techniques and Instrumentation for Atmospheric and Space Research III* (pp. 277–288). Denver, CO, United States: SPIE. https://doi.org/10.1117/12.366382

Shefov, N. N. (1968). Intensity and rotational temperature variations of hydroxyl emission in the night-glow. *Nature*, *218*(5148), 1238–1239. https://doi.org/10.1038/2181238a0

Shefov, N. N. (1969). Hydroxyl emission of the upper atmosphere—I: The behaviour during a solar cycle, seasons and geomagnetic disturbances. *Planet. Space Sci.*, *17*(5), 797–813. https://doi.org/10.1016/0032-0633(69)90089-0

Sun, M., Li, Z., Li, J. Y., Lu, J. Y., Gu, C. L., Zhu, M. B., and Tian, Y. F. (2022). Responses of mesosphere and lower thermosphere temperature to the geomagnetic storm on 7–8 September 2017. *Universe*, *8*(2), 96. https://doi.org/10.3390/universe8020096

von Savigny, C., Sinnhuber, M., Bovensmann, H., Burrows, J. P., Kallenrode, M. B., and Schwartz, M. (2007). On the disappearance of noctilucent clouds during the January 2005 solar proton events. *Geophys. Res. Lett.*, *34*(2), L02805. https://doi.org/10.1029/2006GL028106

Wand, R. H. (1983). Lower thermospheric structure from millstone hill incoherent scatter radar measurements: 2. Semidiurnal temperature component. *J. Geophys. Res.: Space Phys.*, *88*(A9), 7211–7224. https://doi.org/10.1029/JA088iA09p07211

Wang, W., Burns, A. G., Wiltberger, M., Solomon, S. C., and Killeen, T. L. (2008). Altitude variations of the horizontal thermospheric winds during geomagnetic storms. *J. Geophys. Res.: Space Phys.*, *113*(A2), A02301. https://doi.org/10.1029/2007JA012374

Yuan, T., Zhang, Y., Cai, X., She, C. Y., and Paxton, L. J. (2015). Impacts of CME-induced geomagnetic storms on the midlatitude mesosphere and lower thermosphere observed by a sodium lidar and TIMED/GUVI. *Geophys. Res. Lett.*, *42*(18), 7295–7302. https://doi.org/10.1002/2015GL064860

Zhang, Y. L., Paxton, L. J., Schaefer, R., and Swartz, W. H. (2022). Thermospheric conditions associated with the loss of 40 Starlink satellites. *Space Wea.*, *20*(10), e2022SW003168. https://doi.org/10.1029/2022SW003168

Zou, Z. C., Xue, X. H., Yi, W., Shen, C. L., Yang, C. Y., Tang, Y. H., Chen, T. D., and Dou, X. K. (2020). Response of the high-latitude upper mesosphere to energetic electron precipitation. *Astrophys. J.*, *893*(1), 55. https://doi.org/10.3847/1538-4357/ab7eb0